



Cite this: DOI: 10.1039/c6lc01075j

## Robust scalable high throughput production of monodisperse drops†

E. Amstad,<sup>ab</sup> M. Chemama,<sup>a</sup> M. Eggersdorfer,<sup>a</sup> L. R. Arriaga,<sup>a</sup> M. P. Brenner<sup>a</sup> and D. A. Weitz<sup>\*ac</sup>

Monodisperse drops with diameters between 20 µm and 200 µm can be used to produce particles or capsules for many applications such as for cosmetics, food, and biotechnology. Drops composed of low viscosity fluids can be conveniently made using microfluidic devices. However, the throughput of microfluidic devices is limited and scale-up, achieved by increasing the number of devices run in parallel, can compromise the narrow drop-size distribution. In this paper, we present a microfluidic device, the millipede device, which forms drops through a static instability such that the fluid volume that is pinched off is the same every time a drop forms. As a result, the drops are highly monodisperse because their size is solely determined by the device geometry. This makes the operation of the device very robust. Therefore, the device can be scaled to a large number of nozzles operating simultaneously on the same chip; we demonstrate the operation of more than 500 nozzles on a single chip that produces up to 150 mL h<sup>-1</sup> of highly monodisperse drops.

Received 26th August 2016,  
Accepted 22nd September 2016

DOI: 10.1039/c6lc01075j

[www.rsc.org/loc](http://www.rsc.org/loc)

## Introduction

Microparticles and microcapsules of a well-defined size and composition are commonly used in the food,<sup>1</sup> pharmaceutical,<sup>2</sup> cosmetic,<sup>3</sup> and oil industries;<sup>4</sup> these particles are often produced using monodisperse drops as templates.<sup>5</sup> The production of drops with a very narrow size distribution requires a tight control over the drop formation. This level of control can conveniently be achieved with microfluidic devices. However, low throughput limits the use of microfluidics to niche applications.<sup>6,7</sup> The only way the production rate can be increased is through parallelization to simultaneously operate a large number of nozzles.<sup>8–17</sup> However, for this to be accomplished requires operation of multiple nozzles in a very robust fashion, where coupling between individual nozzles is minimized, where the drop size distribution is insensitive to any variations in flow conditions, and where the throughput of individual nozzles is as high as possible. These constraints de-

mand tight control over the mechanism of drop formation. One robust method to control drop formation is through the use of flow focusing. However, in this case, the drop size depends on the fluid flow rate, making large-scale parallelization difficult. This difficulty can be alleviated if the design of the nozzle is optimized such that the dependence of the drop size on the fluid flow rates is much weaker.<sup>18</sup> Nevertheless, even with optimized nozzles, the drop size remains dependent on fluid flow rates. Moreover, flow focusing requires additional channels for the flow of the continuous phase adjacent to each nozzle, thereby increasing the volume of a single nozzle and ultimately limiting the throughput.<sup>8,10</sup> The requirement for flow of the continuous phase can be eliminated by making drops using a step at the outlet of the nozzle to form them through a gradient in the Laplace pressure between the incoming fluid and the drop.<sup>15,16,19–22</sup> These step emulsification devices can operate with high throughputs and produce drops of a controlled size.<sup>15,16,21,23</sup> However, their size distribution is usually significantly broader than that of drops produced in microfluidic flow focusing devices under optimized conditions. This limitation can be overcome by replacing the step with a more gradual, continuous change in height.<sup>14</sup> However, while very monodisperse drops are produced, the flow rate is restricted because fluid flow is driven by small gradients in Laplace pressure, limiting the throughput. Thus, production of monodisperse drops with diameters exceeding 10 µm at high throughput requires an improved control over drop formation in a fashion that can be

<sup>a</sup> School of Engineering and Applied Sciences, Harvard University, Cambridge, Massachusetts 02138, USA. E-mail: weitz@seas.harvard.edu

<sup>b</sup> Institute of Materials, Ecole Polytechnique Fédérale de Lausanne (EPFL), Switzerland

<sup>c</sup> Department of Physics, Harvard University, Cambridge, Massachusetts 02138, USA

† Electronic supplementary information (ESI) available: Additional optical micrographs of another nozzle, the influence of the device height on the maximum throughput, and calculations of the drop precursor shape. See DOI: 10.1039/c6lc01075j

easily scaled. Such a device could significantly broaden the utility of microfluidics for drop production, well beyond niche applications.

In this paper, we present a parallelized microfluidic device, the millipede device, which produces monodisperse drops with diameters between 20  $\mu\text{m}$  and 160  $\mu\text{m}$  using a nozzle that is triangular in its shape with its cross-section gradually increasing until it reaches a step where the channel height abruptly changes. This nozzle results in drop formation through a static instability that is determined solely by the device geometry. This instability determines the volume of fluid that is pinched off, which is, hence, the same every time a drop forms. As a result, the drop size is determined solely by the device geometry, independent of fluid properties and flow rates, making operation of the device very robust. We demonstrate the simultaneous operation of 550 individual nozzles in parallel to produce highly monodisperse drops, with diameters ranging from 20  $\mu\text{m}$  to 160  $\mu\text{m}$  with coefficients of variations as low as 3%, at a throughput up to 150 mL per hour. Moreover, if drop-size variations of up to 5% can be tolerated, the throughput can reach 700 mL per hour and device.

## Results and discussion

The millipede device is made from poly(dimethyl siloxane) (PDMS) using soft lithography.<sup>24</sup> It contains hundreds of in-

dividual nozzles located on each of two long sides of a central channel. These nozzles connect the central channel to two collection channels, as shown schematically in Fig. 1A. The inner phase flows through the central channel and infuses into the outer phase through each of the nozzles, as shown in the optical micrograph in Fig. 1B. Each nozzle contains a triangular reservoir at its end, just before it joins the collection channel, as shown in the optical micrograph in Fig. 1C. The channel height increases abruptly by more than an order of magnitude, where the nozzle meets the connection channel at the end of the reservoir, as depicted schematically by the cross-section of a nozzle shown in Fig. 1D. Drops form in the collection channels at these steps and are collected through a single outlet located downstream of the device, as shown in Fig. 1A.

Operation of the millipede device requires that the channel walls be strongly preferentially wet by the outer phase. Here, we focus on aqueous drops dispersed in an outer phase composed of a fluorinated oil and thus, we make the channel walls fluorophilic by treating them with a fluorinated oil (HFE7500) containing 1 vol% fluorinated trichlorosilane. This treatment can easily be modified to change the wettability of the device as required by the nature of the fluids. For example, to make aqueous drops in hydrocarbon oil we treat the channel walls with trichlorododecylsilane or to make oil drops in an aqueous solution we treat the channel walls with polyelectrolytes.<sup>25</sup>

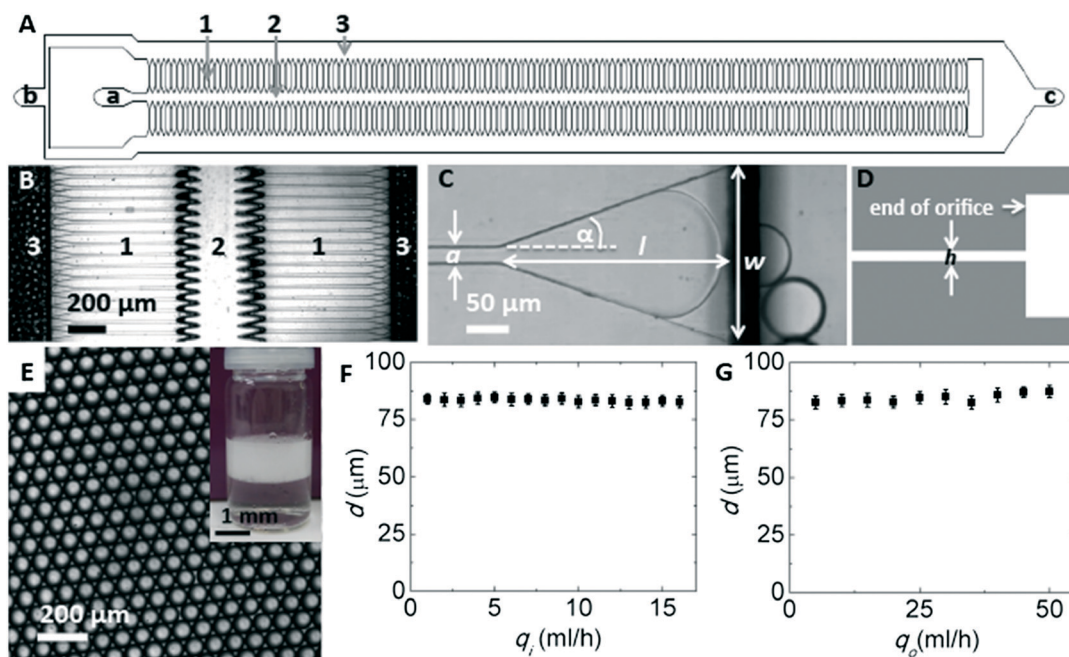


**Fig. 1** (A) Schematic illustration of the millipede device with the (1) nozzles, and the channels for the (2) inner and (3) outer phases. The inner phase is injected through inlet (a), the outer phase through inlet (b), and drops are collected at the outlet (c). (B) Optical micrograph of a section of the millipede device in operation, showing its nozzles (1), and channels for the inner (2) and outer phases (3). (C) Optical micrograph of a single nozzle. The connecting channel has a width,  $a$ , and leads into the reservoir of length,  $l$ , opening angle,  $\alpha$ , and width at the step,  $w$ . (D) Cross-section of a nozzle of height,  $h$ , showing the step at the end of the reservoir. (E) Optical micrograph of drops produced at a flow rate of the inner phase of  $q_i = 20 \text{ mL h}^{-1}$  and that of the outer phase was  $q_o = 30 \text{ mL h}^{-1}$ . Inset: Amount of drops produced within 30 s. (F and G) The diameter of drops produced in a device with 550 nozzles and  $h = 20 \mu\text{m}$  as a function of (F)  $q_i$  for  $q_o = 20 \text{ mL h}^{-1}$  and (G) as a function of  $q_o$  for  $q_i = 5 \text{ mL h}^{-1}$ .

To demonstrate the operation of the millipede device, we use one that has 550 nozzles, each of which has a height,  $h$ , of 20  $\mu\text{m}$  and has a reservoir that has a length,  $l$ , of 330  $\mu\text{m}$  with an opening angle,  $\alpha$ , of 19°, as shown in Fig. 1. We use an inner phase consisting of an aqueous solution of 20 wt% poly(ethylene glycol) (PEG,  $M_w = 6 \text{ kDa}$ ) to increase the viscosity to 8 mPa s. We use an outer phase consisting of a fluorinated oil containing 1 wt% of a fluorinated surfactant<sup>26</sup> to stabilize the drops, whose viscosity is 1 mPa s. We inject the inner phase at a flow rate,  $q_i = 15 \text{ mL h}^{-1}$  and the outer phase at a flow rate,  $q_o = 20 \text{ mL h}^{-1}$ ; hence the volume fraction of the resulting drops is 40%, much higher than values achieved with flow focusing devices. The resultant drops have an average size of 75  $\mu\text{m}$  and a very narrow size distribution, as shown on the optical micrograph in Fig. 1E. The coefficient of variation of the drop size, CV, defined as the standard deviation of the drop size distribution divided by the average drop size, is as low as 3%.

To determine the origin of the very narrow drop size distribution, we measure the drop size as a function of the fluid flow rates. The size of drops produced in the millipede device is independent of the fluid flow rates: the drop size remains unchanged if we vary the flow rate of the inner phase between 1 and 16  $\text{mL h}^{-1}$ , while holding  $q_o$  fixed at 20  $\text{mL h}^{-1}$ , as shown in Fig. 1F. Similarly, the drop size remains unchanged if we vary the flow rate of the outer phase between 5 and 50  $\text{mL h}^{-1}$  while holding  $q_i$  fixed at 5  $\text{mL h}^{-1}$ , as shown in Fig. 1G. The drop size also remains unchanged if we tilt the device by 90° along its long axis, indicating that it is independent of gravity. This behavior is similar to that observed for devices where fluid flow is driven by Laplace pressure gradients.<sup>14–16,22,23,27–29</sup> However, it is in stark contrast to flow-focusing drop-making geometries where the drop size is strongly flow-rate dependent, resulting in broader size distributions, as variations in the flow rate of individual drop makers are inevitable.<sup>10,30–33</sup> This broadening is exacerbated if any of the channels clog during the operation.

To investigate the nature of the drop formation, we visualize the flow in the nozzle using a high-speed camera, operated at 10 000 frames per second. During the initial stages of

drop formation, the inner phase forms a tongue with a semi-circular leading edge, as shown in the optical micrograph in Fig. 2A. As soon as the tongue crosses the step and enters the tall collection channel, a drop forms and grows rapidly, draining the tongue in the reservoir and making it diamond-shaped, as shown in the time-lapse optical micrographs in Fig. 2B–E. Ultimately, the drop detaches and the liquid in the reservoir retracts, as shown in Fig. 2F, whereupon it again forms a semi-circular leading edge, and begins to form the tongue to start formation of the next drop.

The triangular reservoir is an essential component of the nozzle. To investigate its role, we add 3  $\mu\text{m}$  diameter polystyrene beads to the inner phase to visualize the fluid flow in the reservoir during drop formation. By following the trajectory of these beads, we observe that the velocity of the water steadily decreases as the cross-section of the reservoir increases; eventually becoming much slower than the velocity in the entrance of the nozzle. However, once the fluid crosses the step and the drop begins to form, the fluid flow rate at the exit of the nozzle increases rapidly as the drop grows, as shown in Movie S1.† Since the injection rate of the fluid at the inlet is constant, the fluid acceleration in the reservoir must be caused by the flow geometry. As the radius of the drop,  $r$ , grows, its internal Laplace pressure,  $L_p = \frac{\gamma}{r}$  decreases; here  $\gamma$  is the interfacial tension. By contrast, the surface curvature of the tongue remains unchanged as its main contribution comes from the curvature in the direction of the nozzle height. Hence, as the drop grows, a gradient in Laplace pressure with the tongue develops, sucking liquid from the reservoir into the drop at a rate that increases as the drop grows, by analogy to step emulsification devices.<sup>19,34</sup> However, the rate of fluid flow into the reservoir is set by the injection rate and does not increase. Therefore, the reservoir de-couples the fluid flow into the growing drop from that of the externally driven flow. This must be a contributing reason for the independence of drop size and fluid flow rates. Moreover, the triangular shape of the reservoir likely facilitates the back-flow of the outer phase, which must occur since the fluid flow out of the reservoir into the drop as it grows is

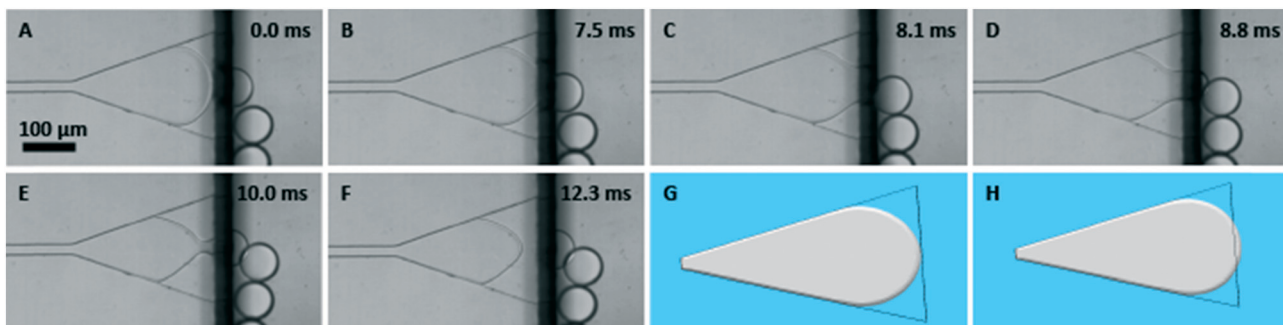


**Fig. 2** (A–F) Time-lapse optical micrographs of drop formation in a millipede device with  $h = 20 \mu\text{m}$ ,  $l = 330 \mu\text{m}$ , and  $\alpha = 19^\circ$ . The black bar is an imaging artefact due to the abrupt change in channel height. The elapsed time is indicated in the upper right corners. (G and H) Surface Evolver simulations of early stages of the drop. Snap shots are taken at an angle to better visualize the drop precursor.

faster than the input fluid flow to the reservoir, as shown in Movie S2.<sup>†</sup> However, because we use an outer phase whose viscosity is always at least three times lower than that of the inner phase, the back-flow of the outer phase into the reservoir is faster than the fluid flow of the inner phase into the drop. Therefore, this back-flow does not influence drop formation in our case.

To explore the break-up of drops we simulate the onset of their formation. Because the fluid velocity where the drop is formed is much slower than the injection velocity, we assume the system to be in a quasi-static state. With this assumption, we can use The Surface Evolver<sup>35</sup> to simulate successive equilibrium shapes of the fluid as the tongue volume increases, by analogy to what has been done for step emulsification processes.<sup>27</sup> The simulated shapes closely resemble those observed experimentally, as shown by comparing the optical micrograph in Fig. 2A and the simulation in Fig. 2G. As the fluid crosses the step, a drop precursor forms, as shown in the simulation in Fig. 2H. When the fluid volume of this drop precursor exceeds a characteristic value, The Surface Evolver no longer finds an equilibrium solution, indicating a transition that designates the beginning of the drop pinch-off.

To examine the nature of the fluid flow before the beginning of the drop pinch-off, we characterize the evolution of the shape of the drop precursor as it grows. As soon as the fluid passes the step, the drop precursor forms and assumes the shape of an ellipsoid that is cut in half along its long axis,  $2a$ . The small axis,  $b$ , is set by the channel height,

$b = \frac{h}{2}$ , as shown in the simulated front and side views in

Fig. 3A and B. As the volume of the drop precursor in-

creases, the long axis of the ellipsoid increases. However, because fluid is pinned at both the top and bottom of the step at the end of the reservoir, the short axis of the ellipsoid remains unchanged as the volume increases, as shown by the evolution of its cross-section in Fig. 3C and by the calculations in the ESI.<sup>†</sup> Once the ratio  $a/b$  reaches some value, The Surface Evolver can no longer find an equilibrium solution, indicating a transition into an out-of-equilibrium state. For devices with  $h = 20 \mu\text{m}$ , our simulations indicate this transition to occur at  $\frac{a}{b} \approx 4.3$ . Interestingly, a Rayleigh-Plateau instability develops when the ratio  $a/b$  exceeds 4.5,<sup>36</sup> and thus this transition must be caused by the formation of a Rayleigh-Plateau instability. However, the instability forms perpendicularly to the fluid flow direction and thus it is the device geometry that determines the most unstable mode; this must scale with  $a$ . Because  $a$  only depends on  $h$ , the wavelength of the instability, which ultimately determines the drop size, depends only on  $h$ . As a result, the drop size is determined purely by the device geometry and is independent of the fluid flow rates.

Because the drop size depends solely on the device geometry, we must determine the scaling of size with the nozzle geometry to allow control of drop size. The volume of the final drop is the sum of the volume of the drop precursor and the additional fluid that flows into the drop until it pinches off. Our simulations show that the diameter and length of the cylindrical drop precursor both scale with  $h$ ; therefore the drop precursor volume scales as  $h^3$ . The additional volume is the product of the pinch-off time and the fluid flux of the inner phase,  $V_a = \tau_p q$ . To determine the scaling of the pinch-off time, we balance the surface tension forces,  $F_\gamma \propto \gamma h$ , and

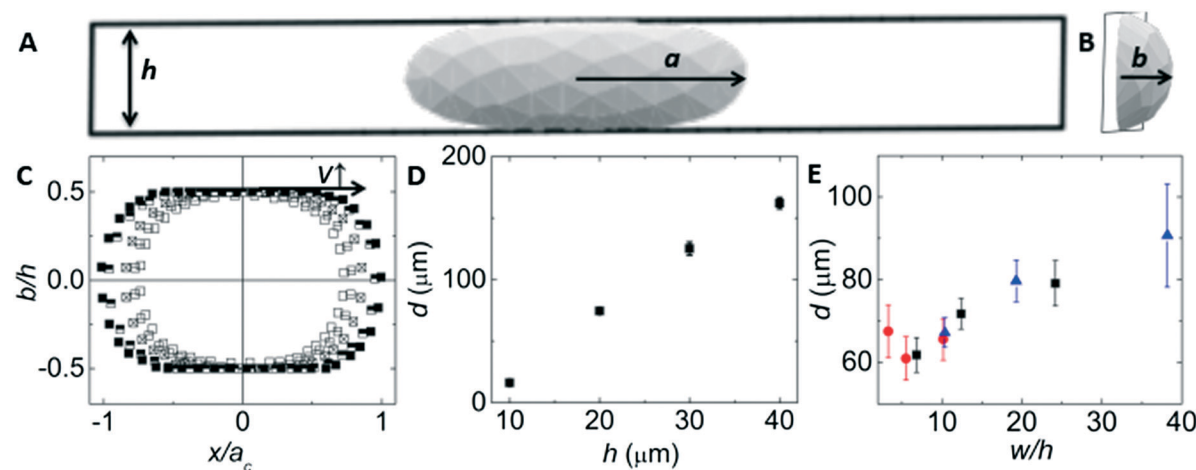


Fig. 3 (A and B) Simulations of the (A) front view and (B) side view of the cylindrical drop precursor with its long axis,  $2a$ , and short axis,  $b = \frac{h}{2}$ . The boxes indicate the end of the reservoir at the step. (C) Evolution of the cross-section of the drop precursor at the exit of the reservoir as its volume,  $V$ , increases. The direction of the volume increase is indicated with a horizontal arrow. (D) Influence of the nozzle height on the drop diameter for an inner fluid with a viscosity of  $3 \text{ mPa s}$ . (E) Influence of the ratio of  $w/h$  on the drop size for reservoirs with  $l = 130 \mu\text{m}$  (●),  $330 \mu\text{m}$  (■), and  $530 \mu\text{m}$  (▲). The error bars indicate the drop size distributions.

viscous forces,  $F_\eta \propto \frac{\eta h^2}{\tau_p}$  and find  $\tau_p \propto h$ ; here  $\eta$  is the viscosity of the inner fluid. We estimate the flux into the growing drop using the Poiseuille law,  $q \sim \frac{\Delta p}{R}$ ,<sup>37</sup> here  $R$  is the hydrodynamic resistance of the reservoir, and  $\Delta p$  is the difference in Laplace pressure in the growing drop and the tongue. Because the growing drop soon has a much larger radius than  $h$ , we ignore its Laplace pressure and approximate  $\Delta p$  to scale with  $h^{-1}$ . We approximate the reservoir as a rectangular channel and thus  $R \propto h^{-3}$ .<sup>37</sup> As a result, the additional volume that flows into the drop scales with  $h^3$ , similar to the drop precursor. Thus the drop diameter scales with  $h$ . To confirm this scaling, we produce drops in devices with  $h$  varying between 10 and 40  $\mu\text{m}$  and measure their sizes using optical microscopy. Indeed, the drop diameter displays a roughly linear scaling with  $h$ , as shown in Fig. 3D. Hence, the drop size can be adjusted by varying  $h$ , which is the dimension that is experimentally the easiest to control precisely. This scaling is distinctly different to that observed in devices with microchannel geometries with terraces where the drop diameter roughly scales with  $h^1$ ,<sup>38</sup> indicating that the drop formation mechanism observed here is distinctly different from that observed in devices whose nozzles contain terraces.

Our simulations predict the drop size to scale with the length of the cylindrical drop precursor; this length increases with increasing width of the reservoir at the step,  $w$ , as detailed in the ESI.† Therefore, we would expect the drop size to also increase with  $w$ . To test this expectation, we vary  $w$  by varying  $\alpha$  between 10° and 35°, keeping the length of the reservoir constant at 330  $\mu\text{m}$  and keeping the height constant at 20  $\mu\text{m}$ . Indeed, the drop diameter increases with increasing  $w$ , as shown by the black squares in Fig. 3E. To vary  $w$  over a

wider range, we fabricate reservoirs with two other lengths, 130  $\mu\text{m}$  and 530  $\mu\text{m}$  and for each length, we test devices with  $\alpha = 10^\circ, 19^\circ$ , and  $35^\circ$ , while keeping the height constant at 20  $\mu\text{m}$ . Indeed, the drop size increases with increasing  $w$ , as shown in Fig. 3E. However, the coefficient of variation of the drop size is independent of  $w$  over a wide range: it is below 5% if drops are produced in reservoirs with a ratio of  $w$  to the height of the device  $5.5 < \frac{w}{h} < 19$ , as indicated by the error bars in Fig. 3E.

The production of drops with a narrow size distribution requires reservoirs to have an optimized ratio of  $w/h$ . In this case, drop precursors can attain a cylindrical shape with  $\frac{a}{b} = 4.5$  such that drop formation is caused by the static instability, resulting in a narrow size distribution, as shown in the optical micrographs in Fig. 4A and B. If this ratio is too low, the size distribution of drops is significantly broadened as exemplified for drops produced in reservoirs with  $\frac{w}{h} = 3.4$ , shown on the optical micrograph in Fig. 4C. We assign this broadening to a change in the mechanism by which drops form: drop precursors formed in these reservoirs cannot attain a cylindrical shape with  $\frac{a}{b} = 4.5$ . Thus, drops cannot be formed by the static instability but must form through a different mechanism. Indeed, the drop forming instability occurs much later, when the volume of the drop is sufficiently large for it to attain a spherical shape. This behavior is highly reminiscent of the traditional, dynamic Rayleigh–Plateau instability that occurs for drop formation in the jetting regime. Hence, there is a lower limit for the ratio  $w/h$ , required for drop formation through the new instability. We

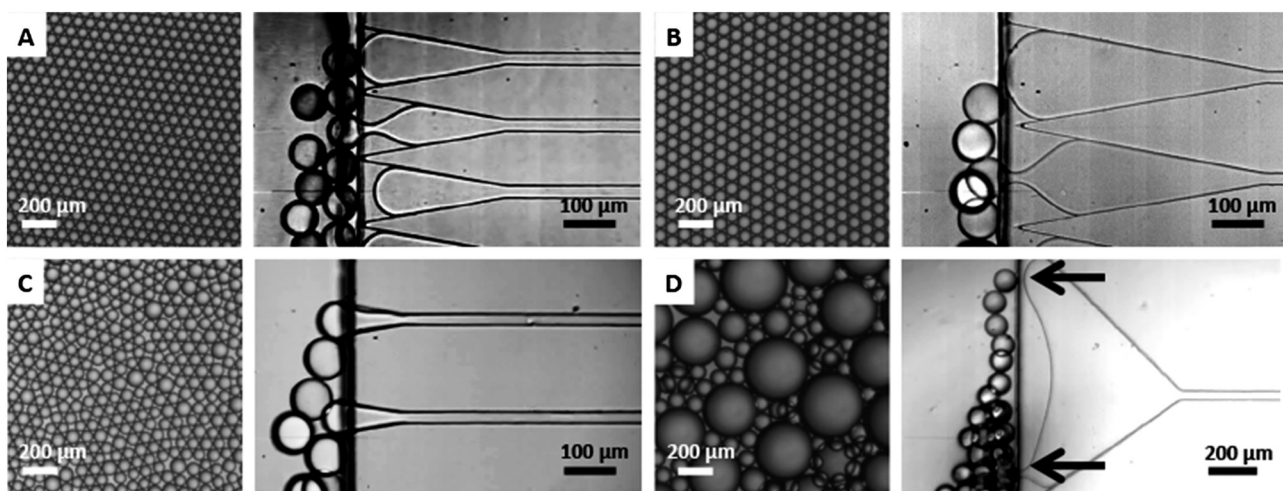


**Fig. 4** Optical micrographs of drops (left) generated in a millipede device (right) with (A–C)  $\alpha = 19^\circ$ , and (D)  $\alpha = 35^\circ$ , and  $l$  is (A) 330  $\mu\text{m}$ , (B and D) 530  $\mu\text{m}$ , and (C) 130  $\mu\text{m}$ . The height of all the devices is 20  $\mu\text{m}$ . (A and B) The reservoirs fulfill the geometric requirements for the new instability to form. (C) The volume of the reservoir is smaller than that of the drops and quasi-static conditions can never be established. Therefore, drops form through a different mechanism that results in a much broader size distribution. (D) The reservoir has a too high ratio of  $w/h$ , such that drops form at multiple locations, resulting in a wide size distribution.

experimentally determine this limit to be  $\frac{w}{h} = 5.5$ , a value, which is only slightly above the predicted value of  $\frac{w}{h} = 4.5$ .

The drop size distribution is also broadened if  $w/h$  becomes too large, as exemplified for a device with  $\frac{w}{h} = 24$  in

Fig. S1.<sup>†</sup> To investigate the reason for this, we further increase  $w/h$  to 35 by increasing the nozzle length to 530 μm; this device produces very polydisperse drops. We monitor the drop formation using a high-speed camera and observe that the mechanism by which drops form is again very different: instead of a single drop forming at the center of the reservoir, two drops are formed at either side. The exact location of the drop formation varies for each drop, resulting in a broad size distribution, as shown in the optical micrograph of Fig. 4D. Hence, there is an upper limit for  $w/h$  beyond which drops form differently. We experimentally determine this upper limit to be  $\frac{w}{h} \approx 19$ . Hence, drops only form through the static instability if  $5.5 < \frac{w}{h} < 19$ .

The static instability described here can only form if the system is in a quasi-static condition, which requires the fluid velocity to be nearly zero. This reduction in the velocity occurs because of the continuously increasing cross-section of the reservoir. Moreover, the reservoir,  $V_{\text{res}}$ , must be sufficient to ensure an adequate decrease in velocity. Remarkably, all drops with a CV below 5% are produced in reservoirs whose volume exceeds the drop volume. By contrast, the volume of

reservoirs with  $l = 130$  μm, and  $\frac{w}{h} = 3.4$ , that produce drops with a CV of 7%, is smaller than the volume of the final drop. In these reservoirs, the deceleration of the fluid velocity is too small to establish quasi-static conditions. Instead, the fluid jets through the orifice and the drop formation mechanism closely resembles that observed in step emulsification devices, as shown in the left optical micrograph of Fig. 4C. These results indicate that the volume of the reservoir must be at least that of the drop for it to be effective in establishing the requisite quasi-static conditions.

A critical feature of the nozzle is the triangular reservoir that extends up to the step; it slows the velocity of the incoming fluid to establish the quasi-static conditions required for drop formation to be initiated through the static fluid instability. Moreover, this triangular shape facilitates the back-flow of the outer phase, which must occur because the fluid flow out of the reservoir into the drop as it grows is faster than the input fluid flow to the reservoir, as shown in Movie S2.<sup>†</sup> However, even with this geometry, drops only form through this static instability if the viscosity of the inner phase is higher than that of the outer phase. In our case, the viscosity of the inner phase is always at least three times higher than that of the outer phase. Hence, the back-flow of the outer phase is never the rate-limiting step and therefore

never influences drop formation. This requirement presents a clear limitation of the device. However, for applications that require drops made of more viscous fluids in a low viscosity fluid, this requirement is actually an important advantage: it facilitates their controlled formation, which is difficult to achieve with standard microfluidic flow focusing devices. This is particularly important when making drops that are used as templates to fabricate microparticles or microcapsules.

The exact shape of the reservoir is quite important for its correct functioning: if we omit the reservoir and instead introduce a straight channel with a rectangular cross-section, drops break up only after the step, by analogy to other step-emulsification devices. If we add a reservoir by abruptly increasing the channel width, drop break-off can occur either at the initial step or at the final opening, as shown in Movies S3 and S4.<sup>†</sup> Hence, the device does not function properly. Instead, it is essential to have a gradual increase in the channel width, resulting in a triangular shaped reservoir.

To increase the throughput of the millipede device, we increase the flow rate of the inner phase. Initially, the frequency of drop formation increases with increasing flow rate, but the drop size remains the same because drops are formed through this static instability. However, on further increase of the flow rate, we ultimately observe a transition from dripping to jetting. We expect this transition to occur when the drop precursor reaches its maximum size before the instability has time to form. This occurs if the injection flow rate exceeds  $\frac{h^3}{\tau_R}$ ; here  $\tau_R$  is the time scale for the Rayleigh Plateau instability to occur. For fluids with viscosities similar to that of water, this time scale is determined by the

balance of inertia and surface tension,  $\tau_R \propto \sqrt{\frac{\rho h^3}{\gamma}}$ ; here  $\rho$  is the density of the inner fluid. Hence, the maximum injection flow rate of the inner phase,  $q_m$ , should scale with  $h^{\frac{1}{2}}$ . To test this prediction, we measure the maximum flow rate of devices with  $h$  between 10 μm and 60 μm, using an inner fluid with a viscosity of 3 mPa s. Indeed, the flow rate at which this transition occurs scales with  $h^{\frac{1}{2}}$ , as shown in Fig. S2.<sup>†</sup> By contrast, this transition is independent of the microchannel geometry for step emulsification devices with terraces,<sup>29</sup> providing further evidence for the different drop break-up mechanism observed here.

There are two time scales that are essential for drop formation: the time required for the Rayleigh Plateau instability to form,  $\tau_R$ , and the time for the drop precursor to grow to its characteristic size,  $\tau_p$ . Drops can only form through this new instability, if  $\tau_R < \tau_p$ . If this is not the case, the elliptical drop precursor continues to grow beyond its characteristic size and if its volume is sufficiently large, it deforms and attains a spherical shape to minimize the interfacial area. In this case, it is no longer the difference in the two lengths of the elliptical precursor drop that drives the Rayleigh–Plateau

instability, and thus drops form by a different mechanism that is similar to that observed in step emulsification. Both these times scale with  $h$ ; however,  $\tau_R$  scales with  $h^{\frac{1}{2}}$ , whereas  $\tau_P$  scales with  $h^3$ . Therefore, if we make  $h$  sufficiently small,  $\tau_P$  always becomes smaller than  $\tau_R$  and the new instability cannot form. Because the drop diameter scales with  $h$ , there must be a lower limit for the diameter of drops that can be produced with the millipede device. By linearly extrapolating the data presented in Fig. 3D, we determine this lower limit to be at  $\approx 6 \mu\text{m}$  for the combination of fluids used here.

Our calculations of  $q_m$  assume the system to be in a quasi-static state such that the formation of the instability is the rate-limiting step. This is the case for fluids with low viscosities that rapidly establish quasi-static conditions during early stages of drop formation. To test if this assumption is applicable also to fluids with higher viscosities, we measure  $q_m$  for inner phases with viscosities ranging from 3 to 30 mPa s. The maximum flow rate at which the millipede device can operate before jetting decreases strongly with increasing viscosity of the inner fluid, as shown for devices with  $h = 20 \mu\text{m}$  by the blue triangles in Fig. 5A. Similar behavior occurs for devices with a larger  $h$ , albeit at higher absolute flow rates, as shown for devices with  $h = 40 \mu\text{m}$  by the black pentagons in Fig. 5A. This decrease in flow rate is a result of changing flow dynamics within the reservoir. For dripping to occur the fluid flow must be quasi-static and the tongue must be semi-circular. During the final stages of drop formation, the shape of the tongue is deformed and becomes diamond like. Thus, it must regain its initial semi-circular form to ensure drop formation through dripping; this is accomplished by the retraction of the fluid back into the reservoir to form the semi-circular shape required for the geometrically controlled instability. As the fluid flow is increased, there is insufficient time for this retraction to occur, and instead, the flow transitions to the jetting regime. The speed of this retraction decreases with increasing viscosity, and thus the maximum throughput also decreases. In this case, the formation of the instability depends on establishing quasi-static flow conditions, and thus  $q_m \propto h^3$ . However, because drops are formed through a static instability, their size is independent of fluid viscosity, as shown in Fig. 5B, in stark contrast to drops formed by in

microchannel devices with terraces<sup>29,39</sup> or straight-through holes.<sup>40</sup>

The main feature of the millipede device is the ease with which hundreds of nozzles can be operated in parallel. To fully exploit this feature, nozzles should be packed at the highest density possible, which requires minimization of the area of their footprint. We approximate the footprint as a rectangle whose length is the sum of the connecting channel and the reservoir. The connecting channel of the nozzle must have a sufficient length to ensure its hydrodynamic resistance is at least 100 times higher than that of the distribution channel; this design condition minimizes differences in fluid flow rates in different nozzles.<sup>8</sup> As a result, the length of the reservoir is much shorter than that of the connecting channel and thus, the length of the nozzle is essentially determined by that of the connecting channel. The width of the rectangular footprint of the nozzle is determined by that of the reservoir at the step, which is the widest point. Thus, the footprint is minimized by using the smallest value of  $w/h$  possible, which is 5.5. To demonstrate the full potential of the millipede device, we use nozzles with reservoirs having  $\alpha = 10^\circ$ ,  $l = 330 \mu\text{m}$ , and

$h = 20 \mu\text{m}$ , resulting in  $\frac{w}{h} = 6.5$ , slightly larger than the

minimum value, and  $\frac{V_{\text{nozzle}}}{V_{\text{drop}}} = 4$ , well above the minimum

acceptable value. The footprint of a single nozzle is  $0.2 \text{ mm}^2$ . We connect 225 nozzles to each side of the distribution channel, resulting in a millipede device containing 550 nozzles. When the areas of the two inlets and one outlet are included, the total footprint is  $250 \text{ mm}^2$ , which is almost 100 times smaller than the footprint of a standard microfluidic flow focusing device containing a single nozzle, two inlets for liquids and one outlet. Moreover, the footprint of a flow focusing device optimized for high throughput applications, with 1000 parallelized nozzles, is  $3000 \text{ mm}^2$ .<sup>41</sup> Hence, the area of a single millipede nozzle is almost 10 times smaller than that of this optimized flow focusing device. Despite of this high nozzle density, we never observe any crosstalk between neighbouring nozzles if drops are formed through the static instability.

One suitable figure of merit for these high throughput drop makers is the volume of drops generated per area and time; this allows direct comparison of the millipede device to other geometries. The maximum throughput is determined by the maximum drop generation frequency of a single nozzle and the packing density of the nozzles. The drop generation frequency in the millipede device is limited by the need to establish quasi-static conditions during early stages of drop formation; it is approximately one order of magnitude lower than that of a single flow focusing drop maker producing drops with a similar size from fluids with a similar viscosity.<sup>42</sup> Nevertheless, because of the high nozzle packing density, the millipede device produces up to 600 liters of drops per hour and  $\text{m}^2$ . This is similar to that of parallelized

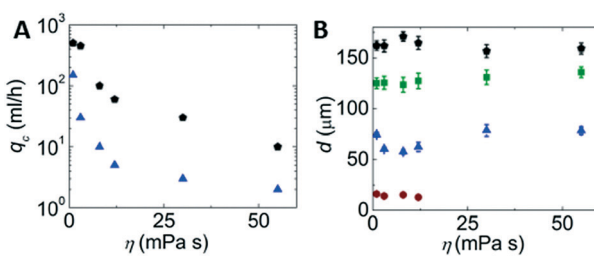


Fig. 5 (A) Influence of the viscosity of the inner phase on its maximum flow rate before the transition into the jetting regime occurs in devices with  $h = 20 \mu\text{m}$  (▲), and  $40 \mu\text{m}$  (●), and 500 individual channels. (B) Size of drops produced in devices with  $h = 10 \mu\text{m}$  (●),  $20 \mu\text{m}$  (▲),  $30 \mu\text{m}$  (■), and  $40 \mu\text{m}$  (●).

**Table 1** Overview over different microfluidic devices

Nozzle geometry	Nozzles per device	Throughput ( $\text{l m}^{-2} \text{ h}^{-1}$ )	Drop diameter ( $\mu\text{m}$ )	CV (%)	Ref.
Triangular (measured)	550	600	75	3	This paper
Triangular (estimated if up-scaled)	550	11 000	75	3	This paper
Wedge	256	3	80	3	14
Terraces	72	0.001	150	4	17
Terraces	1500	1	10	4	43
EDGE (measured)		400	28	5	16
EDGE (estimated if up-scaled)		25 000	9	5	16
Straight-through holes	12 000	1	10	5	44
Straight-through holes	24 772	1	7	4	45
Straight-through holes	4300	60	40	3	22
Straight-through holes	11 224	750	50	2	40
Straight-through holes	23 348	2700	30	20	23

flow focusing devices,<sup>41</sup> however, the coefficient of variation of drops produced in millipede devices is two times lower. Moreover, this throughput is similar to highly parallelized step emulsification devices, as summarized in Table 1. However, none of these highly parallelized devices have nozzles whose volume exceeds that of the drops and thus they never establish quasi-static conditions during initial stages of drop formation. Hence, in their case, the wavelength of the most unstable mode of the instability is not determined solely by the nozzle height<sup>38</sup> but also depends on the fluid properties.<sup>29,34,39,40</sup>

Even higher throughputs can be achieved if nozzles are arranged into a membrane-like structure. For example, devices with straight channels leading into a large reservoir can produce drops at throughputs as high as 6000 liters per hour and  $\text{m}^2$ ,<sup>40</sup> as summarized in Table 1. To compare throughputs to these membrane devices, we assume that the millipede device is stacked in the third dimension to form a membrane. Although we have not done this, it is certainly feasible. To make a comparison to the membrane devices we assume the spacing between adjacent rows of nozzles in a stacking of millipede devices must be at least 1.5 times the diameter of a drop, and, for this comparison, we take it to be 150  $\mu\text{m}$ . We also assume the nozzles to be placed only on one side of the central channel to more closely mimic a membrane geometry. In this case, millipede devices arranged

into a membrane structure would produce 11 000 liters of drops per hour and  $\text{m}^2$ . This is significantly higher than membrane devices with straight holes that produce drops with a similarly small CV, as summarized in Table 1.

Interestingly, under some conditions it is possible to significantly increase the throughput of the millipede device by operating it in the jetting regime, while still retaining a relatively narrow size distribution of the drops. We illustrate this behavior using a device containing 550 nozzles, each one having  $\alpha = 10^\circ$ ,  $h = 40 \mu\text{m}$ , and  $l = 330 \mu\text{m}$ . We use an aqueous solution containing 20 wt% PEG as the inner phase and a perfluorinated oil, containing 1 vol% surfactant, as the outer phase. If the inner phase is injected at flow rates below 150  $\text{mL h}^{-1}$ , the device operates in the dripping regime. Under these conditions, the drop size is independent of flow rates. However, as the flow rates increases, the drop size becomes weakly dependent on  $q_i$ , increasing by 20% as  $q_i$  increases to 700  $\text{mL h}^{-1}$ , as shown in Fig. 6A. Remarkably however, the drop size distribution remains very narrow; an example for drops produced at  $q_i = 600 \text{ mL h}^{-1}$  is shown by the optical micrograph in Fig. 6B. However, the behavior of the device in this high flow rate regime is significantly different: drops are formed in the jetting regime and because of the high density of the channels, the break-up depends on the collective behavior of all the nozzles. The flow of the drops from the neighboring nozzles shears off the growing drop in each

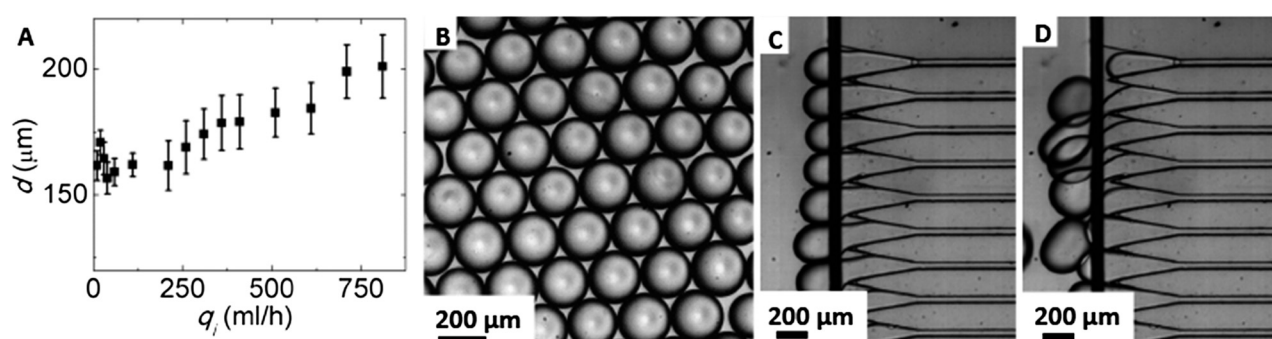


**Fig. 6** (A) Influence of the flow rate of the inner phase on the size of drops formed in devices with  $h = 40 \mu\text{m}$ . (B) Optical micrograph of drops produced in a millipede device with  $h = 40 \mu\text{m}$ . The viscosity of the inner phase is 3 mPa s,  $q_i = 600 \text{ mL h}^{-1}$ , and  $q_o = 700 \text{ mL h}^{-1}$ . (C and D) Optical micrographs (C) before and (D) while drops are sheared off.

nozzle, as shown in the time-lapse optical micrographs in Fig. 6C and D. This class of operation allows the millipede device to function at much higher flow rates; however, this behavior is strictly limited to cases where the viscosity of each fluid is below 5 mPa s, which is five times the viscosity of water. If these conditions are fulfilled, the millipede device produces drops with a very narrow size distribution at throughputs up to 3200 liters per hour and  $\text{m}^2$ , a throughput significantly higher than that reported for drops of similar size with a similarly narrow size distribution produced with any other microfluidic device.

## Conclusions

An important feature of the millipede device is the design of its nozzles: each one contains a triangular reservoir that allows sufficient fluid to be collected for the production of each drop, slowing down the fluid flow, and establishing quasi-static conditions, required for the static instability that leads to drop formation. Because this instability depends only on device geometry, the drop size is independent of fluid injection rates. This makes the device very robust and enables massive parallelization of the nozzles. As a result of the robustness, even a very uncontrolled operation using manually driven syringes is possible; this allows the use of the millipede device for rapid generation of monodisperse drops even in the absence of pumps or other means for controlling the fluid flow for example using only hand-held devices.

One of the most important features of the millipede device is the ability to increase the number of parallelized nozzles to produce drops at very high throughput while retaining a very narrow size distribution. The millipede devices themselves could also be operated in parallel by using larger distribution channels to connect the inlets and outlets. For example, a typical millipede device, such as the one containing 550 nozzles shown in Fig. 1, has dimensions of 44 mm  $\times$  5.6 mm  $\times$  0.4 mm; thus, its volume is 0.1 mL and up to 10 000 of them could be packed into a volume of one liter or one  $\text{dm}^3$ . If operated in the dripping regime, such an array would produce 40 liters of 15  $\mu\text{m}$ -diameter drops per hour and up to 800 liters of 160  $\mu\text{m}$ -diameter drops per hour. Moreover, if operated in the jetting regime, this array would produce as much as 4700 liters of 260  $\mu\text{m}$ -diameter drops. These numbers make it conceivable to produce several thousand tons of highly monodisperse drops per year using a microfluidic device whose volume is only one liter. Thus, the millipede device has the potential to make microfluidics truly useful on a large scale, well beyond scientific applications.

## Acknowledgements

We would like to thank Ken Brakke for his help with The Surface Evolver and Alice Conte for her experimental help. This work was supported by the National Science Foundation (DMR-1310266) and the Harvard Materials Research Science and Engineering Center (DMR-1420570). MC and MPB were

supported by NSF-DMS1411694. MPB is an investigator of the Simons Foundation.

## Notes and references

- B. N. Estevinho, F. Rocha, L. Santos and A. Alves, *Trends Food Sci. Technol.*, 2013, 31, 138–155.
- J. Renukuntla, A. D. Vadlapudi, A. Patel, S. H. S. Boddu and A. K. Mitra, *Int. J. Pharm.*, 2013, 447, 75–93.
- A. Ammala, *Int. J. Cosmet. Sci.*, 2013, 35, 113–124.
- A. Abbaspourrad, N. J. Carroll, S.-H. Kim and D. A. Weitz, *Adv. Mater.*, 2013, 25, 3215–3221.
- S. S. Datta, A. Abbaspourrad, E. Amstad, J. Fan, S. H. Kim, M. Romanowsky, H. C. Shum, B. J. Sun, A. S. Utada, M. Windbergs, S. B. Zhou and D. A. Weitz, *Adv. Mater.*, 2014, 26, 2205–2218.
- A. S. Utada, A. Fernandez-Nieves, H. A. Stone and D. A. Weitz, *Phys. Rev. Lett.*, 2007, 99, 094502.
- P. Garstecki, M. J. Fuerstman, H. A. Stone and G. M. Whitesides, *Lab Chip*, 2006, 6, 693.
- M. B. Romanowsky, A. R. Abate, A. Rotem, C. Holtze and D. A. Weitz, *Lab Chip*, 2012, 12, 802–807.
- M. K. Mulligan and J. P. Rothstein, *Microfluid. Nanofluid.*, 2012, 13, 65–73.
- D. Conchouso, D. Castro, S. A. Khan and I. G. Foulds, *Lab Chip*, 2014, 14, 3011–3020.
- T. Femmer, A. Jans, R. Eswein, N. Anwar, M. Moeller, M. Wessling and A. J. C. Kuehne, *ACS Appl. Mater. Interfaces*, 2015, 7, 12635–12638.
- W. Li, J. Greener, D. Voicu and E. Kumacheva, *Lab Chip*, 2009, 9, 2715–2721.
- T. Nisisako, T. Ando and T. Hatsuzawa, *Lab Chip*, 2012, 12, 3426–3435.
- R. Dangla, S. C. Kayi and C. N. Baroud, *Proc. Natl. Acad. Sci. U. S. A.*, 2013, 110, 853–858.
- S. Sugiura, M. Nakajima, J. H. Tong, H. Nabeta and M. Seki, *J. Colloid Interface Sci.*, 2000, 227, 95–103.
- S. Sahin and K. Schroen, *Lab Chip*, 2015, 15, 2486–2495.
- F. Schuler, N. Paust, R. Zengerle and F. von Stetten, *Micromachines*, 2015, 6, 1180–1188.
- F. Dutka, A. S. Opalski and P. Garstecki, *Lab Chip*, 2016, 16, 2044–2049.
- Z. Li, A. M. Leshansky, L. M. Pismen and P. Tabeling, *Lab Chip*, 2015, 15, 1023–1031.
- N. Mittal, C. Cohen, J. Bibette and N. Bremond, *Phys. Fluids*, 2014, 26, 082109.
- F. Schuler, F. Schwemmer, M. Trotter, S. Wadle, R. Zengerle, F. von Stetten and N. Paust, *Lab Chip*, 2015, 15, 2759–2766.
- I. Kobayashi, M. Nakajima and S. Mukataka, *Colloids Surf. A*, 2003, 229, 33–41.
- G. T. Vladislavljevic, I. Kobayashi and M. Nakajima, *Microfluid. Nanofluid.*, 2011, 10, 1199–1209.
- Y. N. Xia and G. M. Whitesides, *Angew. Chem., Int. Ed.*, 1998, 37, 551–575.
- W.-A. C. Bauer, M. Fischlechner, C. Abell and W. T. S. Huck, *Lab Chip*, 2010, 10, 1814–1819.

- 26 C. Holtze, A. C. Rowat, J. J. Agresti, J. B. Hutchison, F. E. Angile, C. H. J. Schmitz, S. Koster, H. Duan, K. J. Humphry, R. A. Scanga, J. S. Johnson, D. Pisignano and D. A. Weitz, *Lab Chip*, 2008, **8**, 1632–1639.
- 27 K. C. van Dijke, K. C. P. G. H. Schroen and R. M. Boom, *Langmuir*, 2008, **24**, 10107–10115.
- 28 S. Sugiura, M. Nakajima and M. Seki, *Langmuir*, 2002, **18**, 5708–5712.
- 29 S. Sugiura, M. Nakajima, N. Kumazawa, S. Iwamoto and M. Seki, *J. Phys. Chem. B*, 2002, **106**, 9405–9409.
- 30 T. Ward, M. Faivre, M. Abkarian and H. A. Stone, *Electrophoresis*, 2005, **26**, 3716–3724.
- 31 C. Cohen, R. Giles, V. Sergeyeva, N. Mittal, P. Tabeling, D. Zerrouki, J. Baudry, J. Bibette and N. Bremond, *Microfluid. Nanofluid.*, 2014, **17**, 959–966.
- 32 N. C. Christov, K. D. Danov, D. K. Danova and P. A. Kralchevsky, *Langmuir*, 2008, **24**, 1397–1410.
- 33 J. Zawala, K. Szczepanowicz and P. Warszynski, *Colloids Surf., A*, 2015, **470**, 297–305.
- 34 R. Dangla, E. Fradet, Y. Lopez and C. N. Baroud, *J. Phys. D: Appl. Phys.*, 2013, **46**, 114003.
- 35 K. A. Brakke, *Exp. Math.*, 1992, **1**, 141–165.
- 36 L. Rayleigh, *Proc. London Math. Soc.*, 1878, **1–10**, 4–13.
- 37 M. J. Fuerstman, A. Lai, M. E. Thurlow, S. S. Shevkoplyas, H. A. Stone and G. M. Whitesides, *Lab Chip*, 2007, **7**, 1479–1489.
- 38 S. Sugiura, M. Nakajima and M. Seki, *Langmuir*, 2002, **18**, 3854–3859.
- 39 K. van Dijke, I. Kobayashi, K. Schroen, K. Uemura, M. Nakajima and R. Boom, *Microfluid. Nanofluid.*, 2010, **9**, 77–85.
- 40 I. Kobayashi, S. Mukataka and M. Nakajima, *Langmuir*, 2005, **21**, 5722–5730.
- 41 H.-H. Jeong, V. R. Yelleswarapu, S. Yadavali, D. Issadore and D. Lee, *Lab Chip*, 2015, **15**, 4387–4392.
- 42 A. S. Utada, L. Y. Chu, A. Fernandez-Nieves, D. R. Link, C. Holtze and D. A. Weitz, *MRS Bull.*, 2007, **32**, 702–708.
- 43 S. Sugiura, M. Nakajima, H. Itou and M. Seki, *Macromol. Rapid Commun.*, 2001, **22**, 773–778.
- 44 I. Kobayashi, Y. Wada, K. Uemura and M. Nakajima, *Microfluid. Nanofluid.*, 2010, **8**, 255–262.
- 45 I. Kobayashi, M. A. Neves, Y. Wada, K. Uemura and M. Nakajima, *Green Process. Synth.*, 2012, **1**, 353–362.

**Supporting information of “Robust scalable high throughput production  
of monodisperse drops”**

Esther Amstad<sup>1,2</sup>, Michael Chemama<sup>1</sup>, Max Eggersdorfer<sup>1</sup>, Laura R Arriaga<sup>1</sup>,  
Michael P. Brenner<sup>1</sup>, David A. Weitz<sup>1,3</sup>

<sup>1</sup> School of Engineering and Applied Sciences, Harvard University,  
Cambridge, Massachusetts 02138, USA

<sup>2</sup> Current address: Institute of Material Science, Ecole Polytechnique Fédérale  
de Lausanne (EPFL), Switzerland

<sup>3</sup> Department of Physics, Harvard University, Cambridge, Massachusetts  
02138, USA

### **Influence of the nozzle geometry**

To test if we can increase the maximum throughput of an individual nozzle by increasing the opening angle of the reservoir,  $\alpha$ , we fabricate a device with  $\alpha = 35^\circ$  and a nozzle length  $l = 330 \mu\text{m}$ , resulting in  $\frac{w}{h} = 24$ . However, drops produced in these devices have a significantly broader size distribution than those produced in devices with smaller opening angles, as shown in Fig. S1.

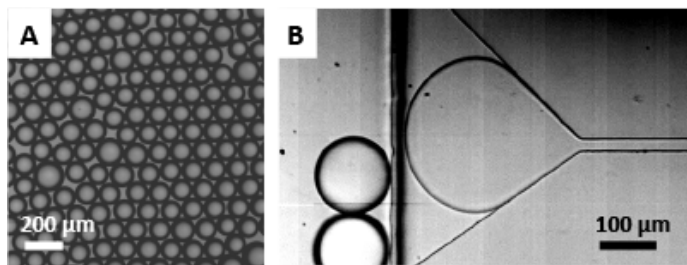


**Figure S1:** Optical micrographs of (a) drops produced in a reservoir with an opening angle,  $\alpha = 35^\circ$  and a length,  $l = 330 \mu\text{m}$  and (b) the drop formation in this reservoir.

### Influence of device height on maximum throughput

If the injection rate of the inner phase is too high, drop production transitions from the dripping into the jetting regime. To quantify the flow rate at which this transition occurs as a function of the nozzle height,  $h$ , we employ a device containing 500 nozzles with  $h$  varying between 10  $\mu\text{m}$  and 60  $\mu\text{m}$ . We produce drops from an aqueous phase containing 10 wt% PEG 6kDa, which has a viscosity of 3 mPas. The maximum flow rate of the inner phase, at which the device can be operated in the dripping regime scales with  $h^{\frac{3}{2}}$ , as derived in the main paper and shown in Fig. S2.

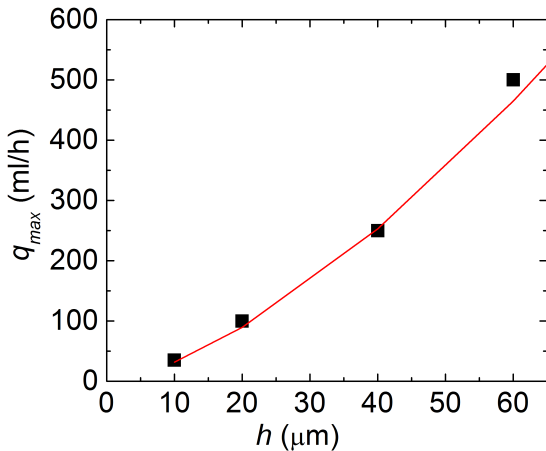


**Figure S2:** Influence of the nozzle height,  $h$ , on the maximum flow rate of the inner phase at which a device with 500 nozzles can be operated in the dripping regime,  $q_{max}$ .

### ***Calculations of the tongue shape***

The fluid adopts a tongue shape inside the reservoir; its radius in the horizontal plane  $R(x_T)$  can be expressed as a function of the device geometry and the fluid contact angle with the walls  $\alpha$ ; here  $x_T$  is the coordinate of the tip of the tongue starting where the cross-section of the nozzle perpendicular to the fluid flow begins to increase and measured on a horizontal axis going through the middle of the drop maker.

Using Figure 1 of the main paper, we can relate  $R(x_T)$  to the device geometry and contact angle:

$$\cos(\alpha - \theta) = \frac{b + x_0 \tan \theta}{R(x_T)} \quad \text{and} \quad R(x_T) \sin(\alpha - \theta) + (x_T - x_0) = R(x_T)$$

Solving for the radius we obtain:

$$R(x_T) = \frac{b + x_T \tan \theta}{\cos(\alpha - \theta) + \tan \theta (1 - \sin(\alpha - \theta))} \quad (1)$$

Once the fluid passes the step and enters the tall collection channel, a drop precursor forms. It is more convenient to parametrize the problem with  $a$ , the semi-major axis of the ellipse than  $x_T$ . They are related by  $x_T = L + R(x_T) - \sqrt{R(x_T)^2 - a^2}$ . Inserting this expression in (1) and solving for  $R(x_T)$ , we get:

$$R(a) = \frac{A(1 - \nu) - \nu \sqrt{A^2 + a^2(2\nu - 1)}}{1 - 2\nu}$$

with

$$A = \frac{b + \tan \theta L}{\cos(\alpha - \theta) + \tan \theta(1 - \sin(\alpha - \theta))} \quad \text{and} \quad v \\ = \frac{\tan \theta}{\cos(\alpha - \theta) + \tan \theta(1 - \sin(\alpha - \theta))}$$

The radius,  $r$ , of the drop precursor, which is equal to the short axis of the ellipsoid, is obtained by imposing the constant mean curvature condition. The mean curvature of the fluid outside the nozzle is  $1/2r$  while inside we have two contributing terms: the curvature in the horizontal plane  $1/R(a)$  and the curvature in the vertical plane  $2 \cos \alpha/h$ , where  $h$  is the height of the nozzle.

$$\frac{1}{r} = \frac{2 \cos \alpha}{h} + \frac{1}{R(a)}$$

For very small drops production, the first term dominates and so  $r \approx h/2 \cos \alpha$ .

At breakup, the drop precursor has the shape of an ellipsoid of radius  $r$  and length  $9r$ , implying a linear scaling for the droplet radius with  $h$ .

**Movie S1:** Formation of aqueous drops in a 330  $\mu\text{m}$  long, 20  $\mu\text{m}$  tall reservoir whose opening angle,  $\alpha$ , is 19°; therefore, the ratio of the width at the step to the height is  $\frac{w}{h} = 12.4$  and  $\frac{V_{res}}{V_{drop}} = 7.3$ . The aqueous phase contains 20 wt% PEG 6 kDa to increase the viscosity and polystyrene beads to visualize the fluid flow. We used fluorinated oil containing fluorinated surfactants as an outer phase. The movie is 100 times slowed down.

**Movie S2:** Formation of aqueous drops in a 330  $\mu\text{m}$  long, 20  $\mu\text{m}$  tall reservoir whose opening angle,  $\alpha$ , is 19°; therefore, the ratio of the width at the step to the height is  $\frac{w}{h} = 12.4$  and  $\frac{V_{res}}{V_{drop}} = 7.3$ . The outer phase contains very small thioglycerol drops that were added to visualize its flow. The movie is 100 times slowed down.

**Movie S3:** Formation of aqueous drop in a 200  $\mu\text{m}$  long, 20  $\mu\text{m}$  tall reservoir whose opening angle is 90°. The flow rate of the inner phase is 5.5 mL/h, that of the outer phase is 20 mL/h. Drops break up at the initial step of the reservoir, which is its entrance. The movie is 10 times slowed down.

**Movie S4:** Formation of aqueous drop in a 200  $\mu\text{m}$  long, 20  $\mu\text{m}$  tall reservoir whose opening angle is 90°. The flow rate of the inner phase is 7 mL/h, that of the outer phase is 20 mL/h. Drops break up after they passed the step, at the final opening of the reservoir. The movie is 10 times slowed down.